AIP | Journal of Applied Physics

Study of generalized magneto-optical ellipsometry measurement reliability

J. A. Arregi, J. B. Gonzalez-Diaz, E. Bergaretxe, O. Idigoras, T. Unsal et al.

Citation: J. Appl. Phys. **111**, 103912 (2012); doi: 10.1063/1.4720471
View online: http://dx.doi.org/10.1063/1.4720471
View Table of Contents: http://jap.aip.org/resource/1/JAPIAU/v111/i10
Published by the American Institute of Physics.

Study of generalized magneto-optical ellipsometry measurement reliability

J. A. Arregi, J. B. Gonzalez-Diaz,[a] E. Bergaretxe, O. Idigoras, T. Unsal, and A. Berger
CIC nanoGUNE Consolider, E-20018 Donostia-San Sebastián, Spain

(Received 24 November 2011; accepted 27 April 2012; published online 25 May 2012)

We present an experimental and theoretical study of the reliability of generalized magneto-optical ellipsometry measurements, investigate its dependence from data set acquisition geometries, as well as investigate the underlying physics of light reflection for magneto-optical materials to explain the observed behavior. Specifically, we compare the use of two different grids of data points and evaluate their reliability and repeatability in a comparative study. We find that the conventionally used square grid is actually not ideal for generalized magneto-optical ellipsometry (GME) measurements and that the also investigated diagonal lattice is clearly superior. These experimental results were reproduced in theoretical calculations of the detection process. The physical origin of this behavior was identified to be related to the "quality" of the individual data points that are included in the data analysis process, with the highest quality data being achieved near the crossed polarizer line, i.e., the region that is more prominently utilized in the diagonal grid approach presented here. These results will help to improve the precision and the data acquisition time of GME measurements. © *2012 American Institute of Physics*. [http://dx.doi.org/10.1063/1.4720471]

I. INTRODUCTION

Generalized magneto-optical ellipsometry (GME)[1,2] has emerged as a powerful tool to obtain optical and magneto-optical constants of magnetic materials with a very high degree of precision as well as magnetization orientations. The underlying magneto-optics of planar structures was theoretically established by Visnovsky *et al.*,[3,4] whose work was based on an extension of the Yeh's formalism.[5] After its first experimental realization,[1] it was initially employed towards the study of diverse magnetization reversal processes.[6–10] Since then, this non-invasive characterization method has been also successfully applied to the study of magneto-optical coupling in ferromagnetic films,[11] the study of spin-polarized electronic states in multiferroic materials,[12] or to determine the field dependent magnetization orientation via 2-dimensional[2] and 3-dimensional[13] vector magnetometry. In addition, this technique has been recently extended to increase its capabilities and possible applications. For instance, temperature-dependent and spectroscopy measurements have been developed by Neuber *et al.*[14,15] in order to resolve the spectral response of spin-polarized carriers and bands, and thus extracting information about how the ferromagnetic state is created. On the other hand, GME has been reformulated in terms of the Mueller matrix approach, giving this technique the potential to include depolarization effects as well.[13,16]

GME is a light reflection technique that uses a sequential set of incoming light polarizations and detection sensitivity settings for the purpose of measuring the entire reflection matrix, which is the maximum available information for any optical experiment with polarization degree conservation. In a typical GME set-up, the corresponding experimental procedure is facilitated by choosing a sequence of polarizer pair orientations, with one polarizer being located in the incoming light beam path, and one in the outgoing one. Compared to other magneto-optical characterization methods, based on the same magneto-optical Kerr effect (MOKE),[17–19] GME has two key advantages: it can measure optical and magneto-optical constants simultaneously, and it allows for vector magnetometry measurements, all with one simple experimental set-up. The price one pays for these fundamental advantages is the fact that the number of measurements needed for GME is far greater than in conventional MOKE experiments, and that the data analysis is more elaborate, simply because the data set contains far more information. Nonetheless, the data analysis allows for automation by means of non-linear curve fitting, although, due to the large number of measurements, GME is inherently slow. Thus, efficient use of measurement time ought to be a crucial aspect of the GME methodology in general and the system performance of individual setups. The question also relates to the physics of light reflection in the presence of magneto-optical effects, and finding experimental conditions, in which these generally small effects produce the largest possible polarization and light intensity changes. To our knowledge, these two interrelated questions have not been addressed so far, which is the motivation for the work presented here. In our study, we investigated the influence of the grid of polarizer pair orientations that are used in GME measurements onto the achieved data reliability. Specifically, we studied two different strategies to collect the GME-data sets. We will show that the reproducibility of the experiment, and in turn, the reliability of the GME measurements depend rather substantially on the shape of the utilized polarizer orientation pair grid. We will present a data acquisition methodology that is improved in comparison to previous works, and we will discuss and explain how this improvement can be understood in terms of the underlying physics of light reflection in the presence of magneto-optical effects.

[a]Electronic mail: j.gonzalez@nanogune.eu.

The manuscript is organized as follows. First, we will describe the experimental setup and methodology used to obtain the GME measurements. Afterwards, we will show and analyze the experimental results of our comparative study using two different shapes for the polarizer orientation pair grid. Finally, Sec. V will be dedicated to compare these experimental studies to numerical simulations of the measurement process for the purpose of elucidating the physical origin of the observed behavior and improved methodology.

II. EXPERIMENTAL SETUP

The GME technique is based on light reflection measurements and can be performed using a simple experimental setup,[1,2] which is schematically shown in Figure 1. The light from a laser source, here a polarization-stabilized He-Ne laser with $\lambda = 632.8$ nm, passes a first rotatable linear polarizer P_1 and reaches the sample under investigation to be measured with an incident angle of approximately 45° with respect to the sample plane. Upon reflection from the sample, the light goes through a second rotatable linear polarizer P_2, after which its intensity is measured by a photo-detector. The sample itself is placed inside the gap of an electromagnet. In our specific case, the magnet generates a magnetic field that lies in the sample plane but is oriented 45° away from the plane of incidence, so that we can obtain at the same time longitudinal and transverse magneto-optical effects, which GME is able to separate. The light intensity that reaches the photo-detector can be calculated so that one is able to obtain an expression of the normalized light intensity change under magnetic state inversion, given by:[1]

$$\frac{\delta I}{I} = 4\frac{B_1 f_1 + B_2 f_2 + B_3 f_3 + B_4 f_4}{I_0 + f_3 + B_5 f_5 + 2B_6 f_4}, \quad f_k = f_k(\varphi_1, \varphi_2). \quad (1)$$

Hereby, I is the average light intensity and δI the light intensity change due to the magnetic state inversion. The B_k parameters are derived from the coefficients of the reflection matrix, whereas f_k are trigonometric functions that depend only on the angular orientation of the two polarizer angles φ_1 and φ_2 that we define here with respect to the s-polarization axis (see Figure 1). I_0 represents the background signal that is independent from the polarizer orientation and magnetic sample state. Further details on the derivation of Eq. (1) can be found in Ref. 1.

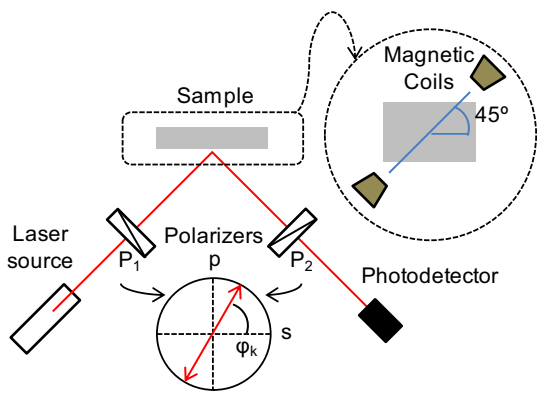

FIG. 1. Scheme of the GME experimental setup and the specific magnet and sample geometry that was utilized in this study.

III. METHODOLOGY

As Eq. (1) implicates, it is generally possible to obtain the reflection matrix from a magnetic sample through multiple independent measurements of the $\delta I/I$ value. Given that the entire optical and magneto-optical information is encoded in six B_k parameters for an arbitrary in-plane magnetization orientation, it is necessary to perform at least six measurements for six different polarizer configurations in order to obtain an independent set of equations. It is, however, much more reliable to measure a far greater number of different polarizer configurations than only six and then determine the B_k from all these $\delta I/I$ data by means of a least-squares fit to Eq. (1). This over-determination furthermore allows checking for the consistency of the data-sets, as well as it enables us to verify that the physics of light reflection is indeed described properly by Eq. (1) for any specific sample. Experimentally, the data sets are acquired by successively modifying the relative orientation of the polarizers and, for every polarizer pair setting, measuring $\delta I/I$ as a function of the magnetic field strength H.[2] By setting different orientations for the polarizers, one is able to construct a grid of $\delta I/I$ data points for each magnetic field value, which is the very data set that is then fitted to Eq. (1) in order to obtain the B_k factors.

In our study, we aim to investigate which set of $\delta I/I$ data points provides more reliable results, and thus represents an efficient way to perform GME measurements. To do so, we compared two different configurations for the polarizer orientation grid. The first one is obtained by taking pairs of polarizer orientations $[\varphi_1, \varphi_2]$ that form a square grid, which is the procedure that was utilized in previous GME-studies.[2] The second one, which to our knowledge has not been utilized so far, consists in a diagonal-shaped grid, which in essence follows the crossed-polarizers line, for which the polarizers keep a relative angular orientation of 90°, irrespective of their absolute orientation in relation to the plane of incidence. These two different configurations are displayed in Figure 2, which also depicts a theoretical color map of the $\delta I/I$ signal for a thin cobalt layer. Both grids have the same overall area and share a common region, but differ in other parts. Overall, the square grid samples more points that are relatively far away from the crossed polarizer line, whereas the diagonal collects more points close to this line.

To compare the reliability of these two different measurement strategies, as well as to understand the physical origin of possible differences, it is insufficient to consider just one measurement set for each type of grid. Instead, the actual measurement repeatability needs to be studied, also because error bars from multi-parameter non-linear fitting procedures are not necessarily indicative of true reliability, since they generally do not include covariance effects. Furthermore, from a purely experimental point of view, it is not possible to know what the measurement-independent "true" values of the B_k parameters are, so that we generally cannot state

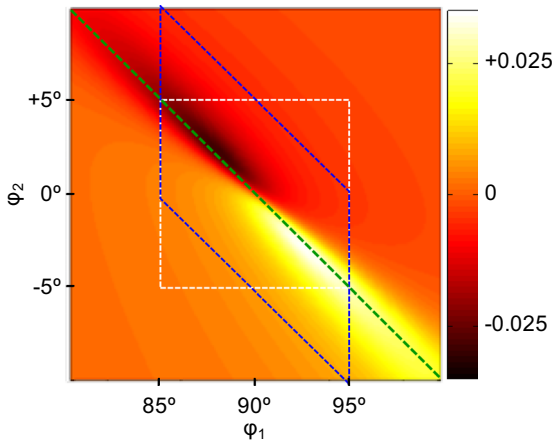

FIG. 2. Illustration of the two different (φ_1, φ_2) grids compared in this study, delimited by dashed lines: square (white dashed line) and diagonal (blue dashed line). The green dashed line defines the crossed-polarizers condition. The color map represents theoretical $\delta I/I$ values for the sample structure employed in the analysis as a function of the two polarizer angles φ_1 and φ_2. The scale represents the intensity of the $\delta I/I$ magnitude.

which grid of data points gives more accurate results. Thus, an experimental investigation only allows us to conclude, which experimental procedure presents a better reproducibility as a quality indicator. It is therefore necessary to carry out a statistically significant experimental study in order to determine which grid presents a narrower distribution of the B_k parameters, and thus, which is the more reliable measurement strategy. This entails the measurement of a very large number of experimental $\delta I/I$ data points, which is very demanding, not only in terms of the time necessary for the measurements but also in terms of the measurement sensitivity to changes in the laser intensity, or drifts of the photo-detector operating point. To avoid these inherent complications, we designed a specific sample and methodology that allowed the collection of a large number of data sets in an efficient manner, as we will explain below in connection with the sample description.

By means of sputter deposition, we fabricated thin Co-films with in-plane uniaxial anisotropy, following the growth sequence of: 75 nm Ag/50 nm Cr/30 nm Co deposited onto HF-etched Si (110) substrates. This specific structure ensures a good epitaxial growth for obtaining Co-films with an in-plane hexagonal closed packed (hcp) c-axis, which is also the easy axis of magnetization.[20] In order to prevent the Co layer from oxidation, the multilayer structure was capped with 10 nm of Ag. As a consequence of its uniaxial in-plane anisotropy, this type of sample exhibits only two magnetization states if the applied magnetic field is oriented along the easy axis. Correspondingly, the magnetization reversal is very sharp in this field direction, only flipping back and forth in between these two magnetization states. In our experimental setup, we oriented the easy axis of magnetization along the field direction, and both at an angle of 45° with respect to the plane of incidence. This magnetization reversal behavior now allows us to obtain a large number of $\delta I/I$ data sets, such as the one indicated in Figure 2, with only one field cycle sequence, because the data sets for different applied field values are statistically independent, but represent the same magnetization state and thus are repeat measurements of each other.

To illustrate this clearly, Figure 3 (top) shows the normalized intensity of the reflected light as a function of the applied magnetic field for a particular orientation of the polarizers ($\varphi_1 = 91°$, $\varphi_2 = 0.5°$). As it can be seen, there exists a high-field range ($|H| > H_c = 320$ Oe) for which the light intensity is constant with the exception of statistical noise. This is precisely because these points represent the same magnetization state due to the saturation of the Co film. Therefore, since these values are directly comparable, we can use this field range to calculate numerous values of $\delta I/I$ as part of the overall $\delta I/I$-maps for different polarizer orientations in just one hysteresis loop measurement. Furthermore, since both branches of the hysteresis loop (shown in black and red, respectively) coincide for fields $|H| > H_c$, it is possible to double the number of independent measurements of $\delta I/I$ for each pair [φ_1, φ_2]. In our experiment, the magnetic field was varied in between ±1000 Oe in steps of

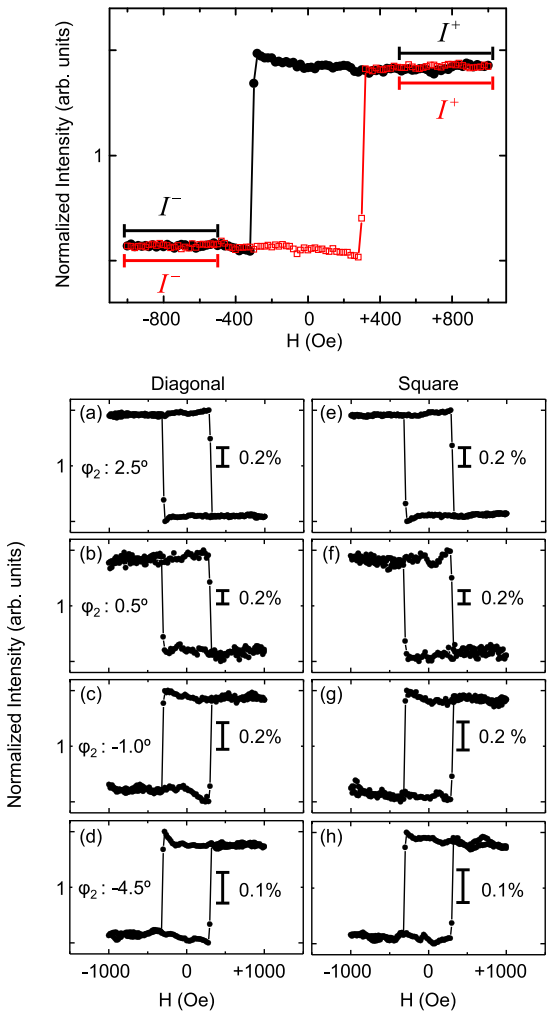

FIG. 3. (Top) Normalized experimental hysteresis loop obtained for a particular polarizers configuration [φ_1, φ_2] = [91.0°, 0.5°]. From this loop, it is possible to calculate several $\delta I/I$ values for the same magnetization state. The lines indicate the utilized data range for our measurements. (Bottom) Normalized experimental hysteresis loops obtained for both types of grids: ((a)–(d)) diagonal; ((e)–(h)) square. The polarizer orientations are common to both, with the first polarizer being fixed to $\varphi_1 = 91°$ in all cases.

20 Oe. The field was strong enough to saturate and reverse our Co-film sample, which was achieved for fields larger than 320 Oe. For our data analysis, we considered only data in the field range $|H| = 500–1000$ Oe to avoid systematic deviations due to possible deviations from exact easy axis and magnetic field alignment. Correspondingly, we acquired 50 $\delta I/I$ values with every measured hysteresis loop, thus, allowing a comprehensive study in a reasonable amount of time. Overall, we performed 2 separate measurements of this sequence for both polarizer orientation grid shapes, so that we generated 100 statistically independent measurements for each grid type.

IV. EXPERIMENTAL RESULTS

The bottom part of Figure 3 shows examples of normalized intensity hysteresis loops retrieved for both types of grids, diagonal ((a)-(d)) and square ((e)-(h)) for different P_2 orientations and a fixed P_1 polarizer orientation of $\varphi_1 = 91°$. The bars in the loops indicate the relative intensity change as a function of the applied magnetic field. It can be observed that, as we decrease the orientation angle of the analyzer, the signal to noise ratio of the loops tends to reduce initially, which is a consequence of the overall low light intensity retrieved by the photo-detector under crossed-polarizers conditions. Upon further decreasing φ_2 and thus surpassing this point, the loops change their sign and an improved signal to noise ratio is observed again. In general, the two series of loops are nearly identical, which is of course related to the fact that they were acquired under nominally identical conditions, which in turn verifies the reproducibility of our measurement conditions.

For each complete GME measurement, we collected hysteresis loops such as the ones shown in Figure 3 for 441 different polarizer pairs. From each of these loops, we extracted a $\delta I/I$ data point at each magnetic field within the saturation range 500–1000 Oe. Thus, for each particular value of the magnetic field, we obtained a set of 441 $\delta I/I$ data points, which can be easily visualized by plotting them into a color map. Examples are shown in Figure 4, where we have depicted four color maps of $\delta I/I$ at the same magnetic field value, two for the square ((a), (b)) and two for the diagonal ((c), (d)) grid of polarizer orientations. Since the signal to noise ratio is high, the maps look virtually identical and do not show any clear visible deviations from each other.

To analyze the measurement reliability and repeatability quantitatively, we have performed least-squares fits to both types of experimental data sets, shown in Figure 4, to Eq. (1), from which we derive the B_k and I_0 as fit parameters.[21] Examples of the achieved fit quality are displayed in Figure 5, where we show two representative experimental $\delta I/I$ maps (Figures 5(a) and 5(c) for the square and diagonal grids, respectively) as well as the corresponding theoretical maps calculated with the parameters obtained from the least-squares fit to Eq. (1) (Figures 5(b) and 5(d)). It can be observed that there is an excellent agreement in between the experiments and the theoretical calculations. The only visible difference is resulting from the fact that the fitted δI/I-maps are plotted on a much denser grid than the experimental data. The value of the coefficient of determination R^2, which describes the overall goodness of a

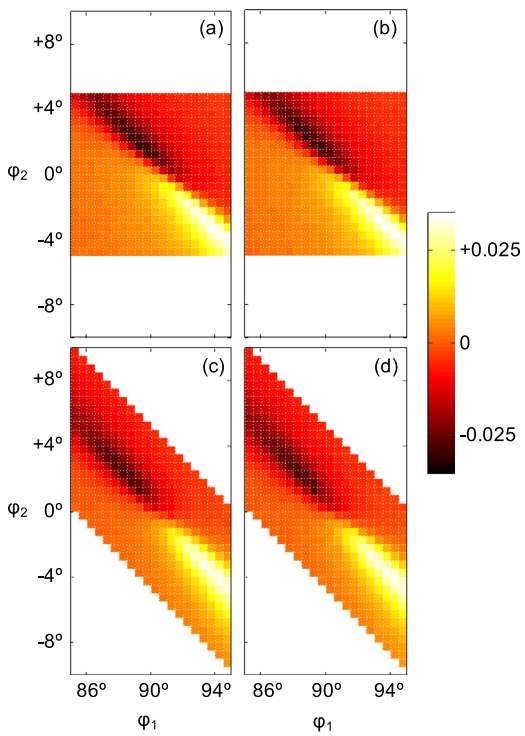

FIG. 4. Examples of experimental $\delta I/I$ maps as a function of the polarizers orientation for both types of grids: square ((a), (b)) and diagonal ((c), (d)). The angular step-width for both polarizers is 0.5° and the color scale is the same for all the maps.

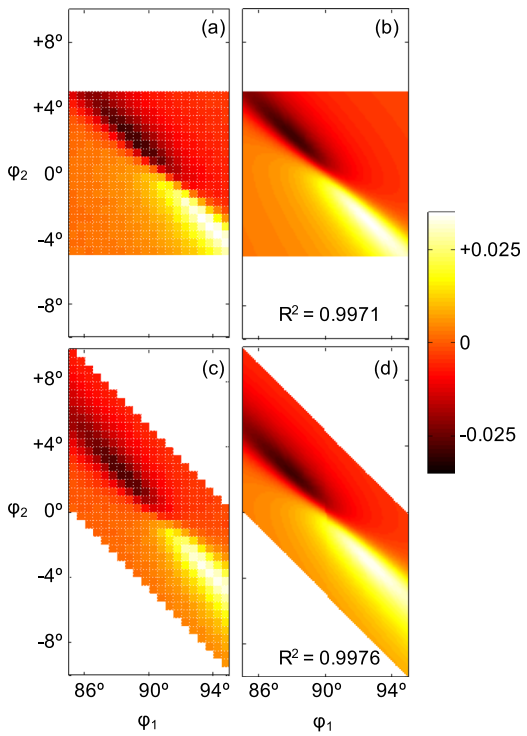

FIG. 5. Left column: examples of experimental $\delta I/I$ maps as a function of the polarizers orientation for both the square (a) and diagonal (c) grids. Right column: (b) and (d) represent $\delta I/I$ maps retrieved as least-squares fits of Eq. (1) to the experimental data. The goodness of the fit is displayed as well.

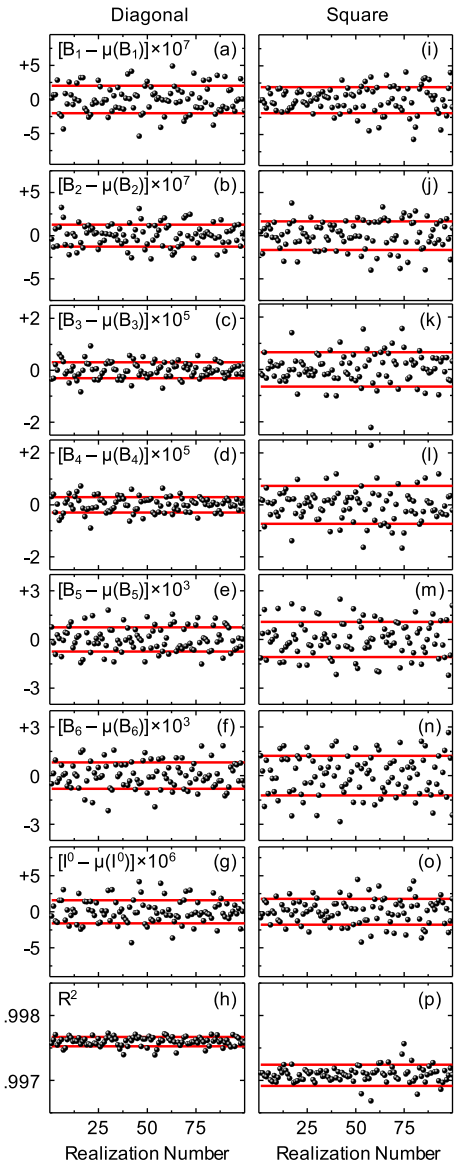

FIG. 6. Least-squares fit results (B_k and I_0) normalized to the mean value for 100 different experimental $\delta I/I$ data sets. The red lines represent the standard deviation of the fit parameters. Left and right columns display the results for diagonal (a–h) and square ((i)–(p)) grids, respectively. The bottom subfigures (h) and (p) show the corresponding values for the coefficient of determination R^2.

least-squares fit, is larger than 0.995 in both cases and thus points to the overall excellent quality of our experimental data sets as well as the validity of Eq. (1).

Figure 6 visualizes the distribution of the B_k and I_0 parameters for the 100 measurements that we conducted under formally identical conditions for both the diagonal and square grids previously described in Figure 2. Specifically, in Figure 6, we plot the individual parameter values normalized to the corresponding mean value $(X_i - \mu(X_i))$ as a function of the measurement number, using the same scale for both grid types. At the bottom of Figure 6, we have also depicted the distribution of the coefficient of determination R^2. The red lines correspond to the standard deviation from the mean value. From this figure, one can see that there are only a few parameters, namely B_1, B_2, and I_0, which show similar standard deviation values for the two different grid types, whereas all other parameters show a clear difference. In all these cases, the standard deviation for the diagonal grid is far smaller than for the square grid, indicating a far superior quality of the measurement repeatability for the diagonal grid approach. In Table I, we have listed the numerical mean and standard deviation values for each parameter and for both grid types. Also the goodness of the least-squares fits as given by R^2 is clearly better for the diagonal grid method when compared to the square one. These results demonstrate that the diagonal grid is less sensitive to the experimental variability such as noise effects, for instance, and thus is much more suitable to perform GME-measurements of high quality for a given number of grid points or measurement time. Correspondingly, the measurement time for GME experiments can be reduced for any fixed value of data quality by following this measurement methodology. This is a key finding of our study.

V. THEORETICAL ANALYSIS

From the experimental data, it is apparent that the diagonal measurement grid produces results that are more reproducible and thus reliable than the previously utilized square grid geometry. However, the experimental data themselves do not reveal in a very direct way why this is the case and what the underlying physics of this measurement behavior is. To elucidate these aspects, we have performed numerical simulations of the measurement process and analyzed the resulting data in the same way, in which we studied the experimental results. For this purpose, we considered a fixed set of B_k values and, from them, calculated δI and I through the respective expressions for the numerator and denominator in Eq. (1). Afterwards, we added a random error to δI and I emulating the signal fluctuations that usually appear in a typical experiment by means of the following expressions:[22]

$$\begin{aligned} I'(\varphi_1,\varphi_2) &= I + \sqrt{I}[-5\times10^{-5} + 10^{-4}\times\sigma_1(\varphi_1,\varphi_2)], \quad \sigma_1 \in [0,1], \\ \delta I'(\varphi_1,\varphi_2) &= \delta I + \sqrt{I}[-5\times10^{-5} + 10^{-4}\times\sigma_2(\varphi_1,\varphi_2)], \quad \sigma_2 \in [0,1], \end{aligned} \tag{2}$$

where σ_1 and σ_2 are variables that randomly vary in the interval [0,1] with constant probability for each polarizer pair. In this way, the $\delta I'/I'$ error is proportional to the square root of the intensity I. We obtained different numerical $\delta I'/I'$ data sets for each grid type, which were subsequently fitted to Eq. (1), in exactly the same way as the experimental data to retrieve

TABLE I. Mean value and standard deviation of the fit parameters (B_k, I_0, and R^2) for 100 different implementations of experimental $\delta I/I$ data sets. Left and right columns display the results for diagonal and square grids, respectively.

	Diagonal		Square	
	μ	σ	μ	σ
B_1	-1.401×10^{-4}	2.00×10^{-7}	-1.377×10^{-4}	1.91×10^{-7}
B_2	8.001×10^{-5}	1.27×10^{-7}	7.761×10^{-5}	1.64×10^{-7}
B_3	2.580×10^{-4}	3.04×10^{-6}	9.926×10^{-5}	6.53×10^{-6}
B_4	-1.683×10^{-4}	2.96×10^{-6}	9.762×10^{-6}	7.28×10^{-6}
B_5	0.9093	7.53×10^{-4}	0.9044	1.08×10^{-3}
B_6	−0.9130	8.09×10^{-4}	−0.9111	1.22×10^{-3}
I_0	2.054×10^{-4}	1.60×10^{-6}	1.961×10^{-4}	1.78×10^{-6}
R^2	0.9976	7.05×10^{-5}	0.9971	1.64×10^{-4}

values for the B_k parameters. For the sake of comparison with the experiment, the theoretical data sets were calculated with exactly the same number of lattice points and angular ranges of polarizer pairs that were used in the experiment.

Figure 7 displays the distribution for each of the B_k parameters and I_0 normalized to their respective mean values as well as the R^2 coefficient for 1000 statistically independent realizations of the $\delta I'/I'$ data set. Left and right columns correspond again to the diagonal and square grids, whereas the red lines denote the standard deviations. The first thing one notices from Figure 7 is that the data dispersion for these numerical data is more pronounced than the one observed experimentally, which simply reflects the fact that the assumed level of noise inserted into the numerical calculations was higher than the actual noise that is present in the experiment. We did this on purpose to emphasize the effects of noise. Similar to what we observed for the experimental results, most of the fitting parameters present a clearly narrower distribution for the diagonal measurement grid than for the square one. The R^2 coefficient also shows smaller point to point deviations as well as an overall improved value for the diagonal grid, in the same way that the experiment did. Table II presents the complete set of values for the input parameters employed in the numerical data set generation, and the mean values and standard deviations of all fitting parameters for both grid types. In addition to the experimental case, Table II also reveals that the diagonal grid results are closer to the exact input parameters than the square grid results. Therefore, there are two key finding here, namely that the numerical data set clearly resemble the behavior of the experimental data and second, that the diagonal grid sets do not only show better repeatability, but also show an improved absolute accuracy as well.

The consistency of the simulated data sets with the experimental results allows us now to investigate the underlying physics of this optical reflection measurement, which causes the superior performance of the diagonal grid case. Bearing in mind that the number of data points is the same for both types of grids, the origin for this improvement must lie in the specific range of polarizer orientations that is different in the data acquisition process. We explored this assumption by numerically analyzing the "quality" of each

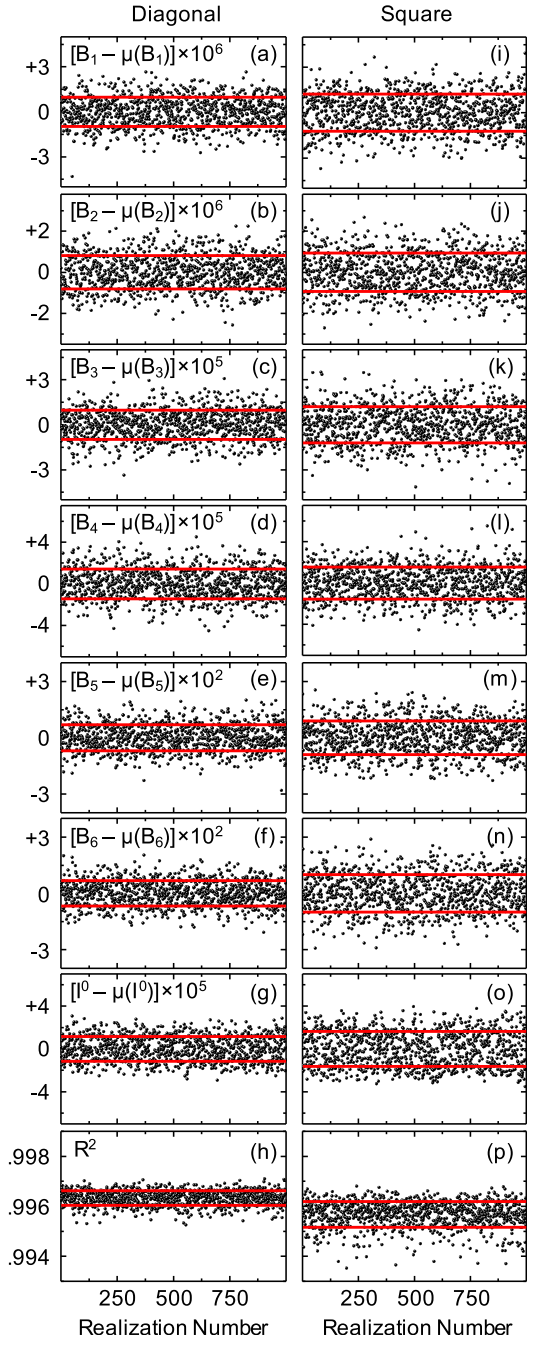

FIG. 7. Least-squares fit results (B_k and I_0) normalized to the mean value for 1000 different theoretical $\delta I'/I'$ data sets. The red lines represent the standard deviation of the fit parameters. Left and right columns display the results for diagonal ((a)–(h)) and square ((i)–(p)) grids, respectively. The bottom subfigures (h) and (p) show the corresponding values for the coefficient of determination R^2.

point in the data sets, meaning that we determined how sensitive the least-squares fit is to the presence or absence of each individual point. To do so, we utilized the coefficient of determination R^2 in defining the sensitivity of the fit to each grid point as the difference between the values for R^2 without such point ($R^2_{without}$) and with it (R^2_{with})

$$S(\varphi_1, \varphi_2) = R^2_{without} - R^2_{with}, \tag{3}$$

where the indices (φ_1, φ_2) represent the polarizer orientation pair, whose significance is being evaluated. Hereby, it is

TABLE II. Mean value and standard deviation of the fit parameters (B_k, I_0, and R^2) for 1000 different implementations of theoretical $\delta I'/I'$ data sets. Central and right columns display the results for diagonal and square grids, respectively, whereas the left column shows the input parameters used in the calculations.

		Diagonal		Square	
	Exact value	μ	Σ	μ	σ
B_1	-1.39×10^{-4}	-1.390×10^{-4}	9.68×10^{-7}	-1.391×10^{-4}	1.22×10^{-6}
B_2	7.88×10^{-5}	7.879×10^{-5}	8.08×10^{-7}	7.886×10^{-5}	9.36×10^{-7}
B_3	1.65×10^{-4}	1.648×10^{-4}	9.71×10^{-6}	1.653×10^{-4}	1.21×10^{-5}
B_4	-5.00×10^{-5}	-4.960×10^{-5}	1.43×10^{-5}	-4.985×10^{-5}	1.55×10^{-5}
B_5	0.907	0.9068	6.98×10^{-3}	0.9067	9.05×10^{-3}
B_6	−0.91	−0.9119	6.82×10^{-3}	−0.9121	9.96×10^{-3}
I_0	2.00×10^{-4}	2.005×10^{-4}	1.16×10^{-5}	2.023×10^{-4}	1.62×10^{-5}
R^2	…	0.9963	2.95×10^{-4}	0.9957	5.20×10^{-4}

important to note that this type of analysis cannot be done by using $\delta I'/I'$ values without any noise, since the removal or addition of any data point would not affect the perfect least-squares fit in either case. Thus, we computed numerical $\delta I'/I'$ maps with random noise implementation according to Eq. (2), in the same way as previously discussed in relation to Figure 7. The fact that noisy data have to be utilized for this analysis, however, causes the analysis of every individual data point to be dependent on the specific noise value that this very data point represents. To suppress this individual noise implementation effect, we performed the calculations according to Eq. (3) several times for every grid point using different specific noise realizations. In our calculations, we found 10 noise realizations for every point sufficient to create a reliable pattern for $S(\varphi_1,\varphi_2)$. The result of this analysis is shown in Figure 8(a). The polarizers range for this map was chosen to include all the grid points within the square and diagonal approach, i.e., $\varphi_1 \in [80^\circ, +100^\circ]$, and $\varphi_2 \in [-10^\circ, +10^\circ]$, in steps of 0.5°. The color scale chosen here is such that a dark color corresponds to a negative value, which in turn means that removing this point will result in a reduction of R^2. Thus, dark colors indicate the particularly valuable or good data points, while bright or white colors, and thus positive S values indicate data points that have just the opposite effect. From the $S(\varphi_1,\varphi_2)$ color map, it can be observed that most of the data points that lie close to crossed polarizer line present a negative value, so that its elimination from the fitting process provides a worse result. On the other hand, the central points, close to complete light extinction, present a positive value that indicates an improvement of the data analysis process when these points are removed. Given these key features, it is easy to see why the diagonal grid presents better results with respect to the square one, since it encompasses more of the most sensitive points.

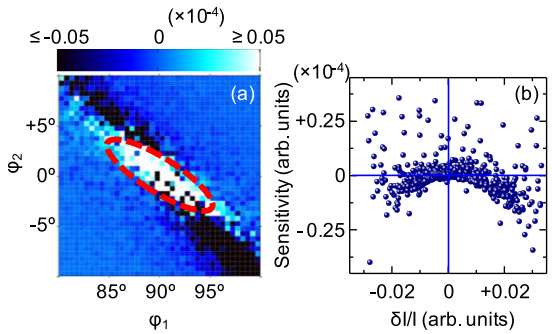

FIG. 8. Sensitivity of the fit quality to the removal of an individual $\delta I'/I'$ data point. A negative value represents a worsening of the fit quality when that point is removed, whereas a positive value represents an improvement. (a) represents the sensitivity as a function of the polarizer orientations whereas (b) represents the same quantity as a function of the $\delta I'/I'$ value. The red dashed ellipse is a guide to the eye and delimits the polarizers region, in which the $\delta I'/I'$ noise is largest and impacting the fit quality negatively.

The vast majority of data points, to which the fit is particularly sensitive, lie near the crossed-polarizers line, where the pure optical reflection is small. In this regime, the reflected light is particularly sensitive to the magneto-optically induced modifications, so that the magnetically induced polarization changes cause the biggest net effect in $\delta I'/I'$ and because of that, these points are the most relevant for the entire ellipsometry measurement. But contrary to this general property of light reflection for ellipsometric purposes, the central points of the sensitivity map show actually the opposite behavior, which is indicated in Figure 8(a) with a red dashed line. This behavior is not immediately evident from Eq. (1), because this equation describes the ideal signal and ignores the existence of noise. However, if one considers the small intensity values in this region, it is evident that these points are very sensitive to noise, so that a rather poor signal to noise ratio for $\delta I'/I'$ is found in this regime. To corroborate this explanation, we compared the correlation between S and $\delta I'/I'$, which is displayed in Figure 8(b). Here, it can be seen that most data tend to condense onto a negative parabola, which means that as $\delta I'/I'$ increases, the sensitivity S improves, i.e., it becomes more negative. Some of the data points in this figure, however, show very poor sensitivity, i.e., positive S values, but instead of being limited to the $\delta I'/I' = 0$ region only, they have nearly random values in the entire $\delta I'/I'$ range. This result indicates that their origin is not correlated with the size of the $\delta I'/I'$ signal, but must have a different cause. A detailed comparison of the data in Figures 8(a) and 8(b) shows that it is exactly the data corresponding to the central white elliptical region in Figure 8(a), which are the randomly distributed positive S values in Figure 8(b) due to their small light intensity I and

corresponding large noise level. Thus, to understand the overall analysis and quality of our data sets, one has to consider both, the magneto-optical signal generation according to Eq. (1) as well as the absolute light intensity and signal level, which reflect not only the fundamental physics of ellipsometric measurements but also the specific detection characteristics of each individual experimental setup. It should also be mentioned that while the map in Figure 8(a) can be considered a first guideline for selecting an ideal set of polarizer pairs, it is not necessarily directly transferable to such a data set optimization, because it is a local sensitivity function that considers the removal of a single data point only. Removal of larger numbers of data points would have to be considered in a collective way due to data point correlations. This optimization problem, however, is beyond the scope of the present work.

VI. CONCLUSIONS

In this study, we have presented an experimental and theoretical study of the efficiency and reliability of the generalized magneto-optical ellipsometry technique, including the investigation of the physical origin that causes different acquisition geometries to behave differently. To our knowledge, this is the first study of its kind, meaning that data set repeatability and efficiency have not been addressed before for GME type measurements. Specifically, we performed an experimental study, in which we compared two different data acquisition schemes, namely, two different grids of data points from which the whole reflection matrix can be retrieved by means of a least-squares fit. For this purpose, we studied the reliability and repeatability of the fitting process on multiple data sets and extracted statistically significant quantities for each one of these grids. We found that the conventionally used square grid is actually not very well suited for GME measurements and that the here investigated diagonal lattice alternative is far superior. These experimental results were reproduced in theoretical calculations of the detection process that also included the leading noise sources of our measurement setup. This theoretical analysis showed furthermore that not only the relative accuracy but also the absolute accuracy is improved for the diagonal grid type. We found out that the physical origin of this improvement was the "quality" of the individual data points that are included in the data acquisition scheme, with the highest quality data being near the crossed polarizer line, while being sufficiently far away from the s-p or p-s extinction condition.

We believe that the findings of this work could also lead to a more general GME sampling optimization, although this goal is not easy to achieve for the following reasons. Firstly, as already mentioned, the quality of the GME data depends on each other, which means that one individually insignificant or even problematic data point might gain substantial relevance if other data points are removed. Secondly, the sensitivity function is usually not known and depends on the reflection matrix itself, which is of course the undetermined goal of the measurement. This means that the optimum region for GME sampling is indeed sample dependent and thus while being close to the crossed polarizers line, it can and will change its size and shape depending on the sample structure or the materials employed. To overcome these problems, one could envision a dynamic data acquisition optimization, in which already acquired partial data sets determine the best possible additional data to be taken next. In any case, the results presented here alone can be employed for an already substantial efficiency increase of the GME technique.

ACKNOWLEDGMENTS

The authors acknowledge funding from the Basque Government under the Etortek Program IE11-304, the Spanish Ministry of Science and Education under Project No. MAT2009-07980, and the European Union under Project No. SOE2/P1/E280. O.I. acknowledges the Basque Government for fellowships (No. BFI09.284) and J. A. A. acknowledges the MICINN for the Formación de Personal Investigador fellowship (No. BES-2010-035194).

[1]A. Berger and M. R. Pufall, Appl. Phys. Lett. **71**, 965 (1997).
[2]A. Berger and M. R. Pufall, J. Appl. Phys. **85**, 4583 (1999).
[3]S. Visnovsky, Czech. J. Phys. Sect., B **36**, 625 (1986).
[4]S. Visnovsky, R. Lopusnik, M. Bauer, J. Bok, J. Fassbender, and B. Hillebrands, Opt. Express **9**, 121 (2001).
[5]P. Yeh, Surf. Sci. **96**, 41 (1980).
[6]O. Idigoras, P. Vavassori, J. M. Porro, and A. Berger, J. Magn. Magn. Mater. **322**, L57 (2010).
[7]A. Tillmanns, S. Oertker, B. Beschoten, G. Güntherodt, C. Leighton, I. K. Schuller, and J. Nogues, Appl. Phys. Lett. **89**, 202512 (2006).
[8]P. Vavassori, M. Grimsditch, V. Novosad, V. Metlushko, and B. Ilic, J. Appl. Phys. **93**, 7900 (2003).
[9]P. Vavassori, M. Grimsditch, V. Novosad, V. Metlushko, and B. Ilic, Phys. Rev. B **67**, 134429 (2003).
[10]M. R. Pufall and A. Berger, J. Appl. Phys. **87**, 5834 (2000).
[11]K. Mok, G. J. Kovacs, J. McCord, L. Li, M. Helm, and H. Schmidt, Phys. Rev. B **84**, 094413 (2011).
[12]M. Bastjan, S. G. Singer, G. Neuber, S. Eller, N. Aliouane, D. N. Argyriou, S. L. Cooper, and M. Rübhausen, Phys. Rev. B **77**, 193105 (2008).
[13]K. Mok, N. Du, and H. Schmidt, Rev. Sci. Instrum. **82**, 033112 (2011).
[14]G. Neuber, R. Rauer, J. Kunze, T. Korn, C. Pels, G. Meier, U. Merkt, J. Bäckström, and M. Rübhausen, Appl. Phys. Lett. **83**, 4509 (2003).
[15]G. Neuber, R. Rauer, J. Kunze, J. Backström, and M. Rübhausen, Thin Solid Films **455**, 39 (2004).
[16]T. Hofmann, U. Schade, C. M. Herzinger, P. Esquinazi, and M. Schubert, Rev. Sci. Instrum. **77**, 063902 (2006).
[17]S. N. Jasperso and S. E. Schnatte, Rev. Sci. Instrum. **40**, 761 (1969).
[18]K. Sato, Jpn. J. Appl. Phys., Part 1 **20**, 2403 (1981).
[19]W. S. Kim, M. Aderholz, and W. Kleemann, Meas. Sci. Technol. **4**, 1275 (1993).
[20]O. Idigoras, A. K. Suszka, P. Vavassori, P. Landeros, J. M. Porro, and A. Berger, Phys. Rev. B **84**, 132403 (2011).
[21]Since the determination of the true s- and p-polarization (as defined by the plane of incidence) in a real laboratory setting is rather imprecise, we introduced two additional fitting factors ($\Delta\varphi_1$ and $\Delta\varphi_2$) in the f_k functions so that the least squares fit could account for the differences in between the φ_1 and φ_2 laboratory and plane-of-incidence reference frames. They present a constant value and have no effect in the present study.
[22]Our measurements as well as any experimental setup have other sources of noise and error than the one we have considered here in our analysis of the measurement process. In particular, random and systematic misalignments of the polarizers, non-ideal polarizer properties, or other effects are always present and could limit the applicability of Eq. (1). However, an analysis of the experimental errors and noise in our system confirmed that signal fluctuations were by far the dominant source of deviations from ideal $\delta I/I$ behavior. For instance, we found them to be at least one order of magnitude higher than the effects of polarizer alignment errors.